

We are IntechOpen, the world's leading publisher of Open Access books Built by scientists, for scientists

6,400

Open access books available

174,000

International authors and editors

190M

Downloads

Our authors are among the

154

Countries delivered to

TOP 1%

most cited scientists

12.2%

Contributors from top 500 universities



WEB OF SCIENCE™

Selection of our books indexed in the Book Citation Index
in Web of Science™ Core Collection (BKCI)

Interested in publishing with us?
Contact book.department@intechopen.com

Numbers displayed above are based on latest data collected.
For more information visit www.intechopen.com



Chapter

Systematic Characterization of High-Dielectric Constant Glass Materials Using THz-TDS Technique

*Osamu Wada, Doddoji Ramachari, Chan-Shan Yang,
Takashi Uchino and Ci-Ling Pan*

Abstract

High-dielectric constant glasses are prerequisite for developing terahertz (THz) components and systems. Oxyfluorosilicate (OFS) glasses have been developed and their THz properties have been characterized by using THz-time domain spectroscopy (THz-TDS) measurements. High-dielectric constant (8–13) and low loss (6–9/cm) properties in the THz region have been demonstrated and their dielectric properties have been studied using the single oscillator-based model through a comparison with other multi-component silicate oxide glasses. Unified single oscillator model, which can distinguish the electronic and ionic contributions to the dielectric property, has been applied in this analysis. The physical origin of the dielectric constant enhancement and the importance of interplay between the electronic polarizability and ionicity in high-dielectric constant glasses have been revealed. This study has demonstrated the usefulness of THz-TDS technique for characterizing dielectric properties of multi-component glasses in detail.

Keywords: terahertz time domain spectroscopy (THz-TDS), dielectric constant, multi-component glasses, electronic/ionic polarizability, polarization ionicity

1. Introduction

Since its early demonstrations in 1980–1990's, terahertz (THz) time-domain spectroscopy (THz-TDS) [1–5] has been employed to study a wide variety of crystalline and non-crystalline materials, e.g., dielectrics [6], semiconductors [7, 8], polymers [9], biological molecules [9], liquid crystals [10], aqueous solutions [11], and many others. The THz-TDS technique has a variety of advantages [9, 11]. For example, a compact system can be built by adopting compact, convenient-to-use components such as photoconductive antenna (PCA) devices as THz sources as well as detectors that can be excited by a sub-picosecond mode-locked laser. Both reflection and transmission configurations can be used depending on the sample nature. Original THz

signal obtained is in time domain, but it can be Fourier transformed into frequency domain over a wide bandwidth. The amplitude and phase information are independently acquired and precise material characteristics can be obtained. Thus, THz-TDS has become a powerful tool for detailed physical/chemical characterization and spectroscopic chemical assessment of materials.

The characteristic vibrational properties of solid materials such as glasses are often found in the THz frequency range (usually 0.1–10 THz). However, glass properties studied so far are limited to some silicate oxide and chalcogenide glasses [12–16]. Some glasses have shown relatively high transparency in the THz frequency range [14–16], and those are potentially useful for the application to a variety of photonic devices, components, and systems in the THz frequency band.

A number of multi-component silicate glasses [17] and various chalcogenide glasses [18] have been developed for optical frequency applications owing to their high chemical/mechanical stability and desirable optical properties such as high refractive index, high transparency, and high optical nonlinearity in visible and mid-infrared wavelength regions. Toward THz applications, further development in glass materials with high-refractive index and low loss is desired. One possibility is oxyfluoride (OF) glasses [19–21], in which non-radiative transitions are suppressed with corresponding high-efficiency luminescence and transparency. Recently, oxyfluorosilicate (OFS) glasses containing metal fluorides have been investigated as they can exhibit combined properties of oxides and fluorides such as a low melting temperature, high chemical/mechanical resistance, low phonon energy, and attractive optical characteristics including high refractive index [19–21]. Multi-component design to increase the electronic and ionic polarizabilities can be useful for realizing high refractive index in the THz frequency range. This also suggests a possibility of high optical nonlinearity in the THz frequency range [22], which is attractive for developing active devices such as switching and wavelength conversion devices. Thus, OFS glasses incorporating appropriate metal oxides/fluorides are expected to provide essential glass materials for THz applications. The THz dielectric properties and their physical nature of such OFS glasses, however, have not been systematically investigated so far.

In the following, we describe the characterization of high-dielectric constant and low loss properties of novel OFS glasses, which are revealed by the application of the THz-TDS technique. First, we describe the THz dielectric properties of two series of multi-component glasses: ZNbKLSNd and PbNKLSNd OFS glasses [23]. Then, we discuss the physical mechanism of the dielectric constant enhancement through a comparative study involving several other multi-component silicate oxide and chalcogenide glasses by using the conventional, simplified single oscillator model [24] and also by developing and applying the more precise, unified single oscillator model [25]. The results show how the dielectric properties of glasses are controlled by the electronic polarizability and ionicity of the glasses, which also demonstrates the usefulness of THz-TDS technique in the glass material characterization.

2. Experimental methods

2.1 THz characterization and analysis techniques

Figure 1 shows the schematic diagram of the transmission-type photoconductive-antenna-based THz-TDS setup employed in this work. Details can be found in our

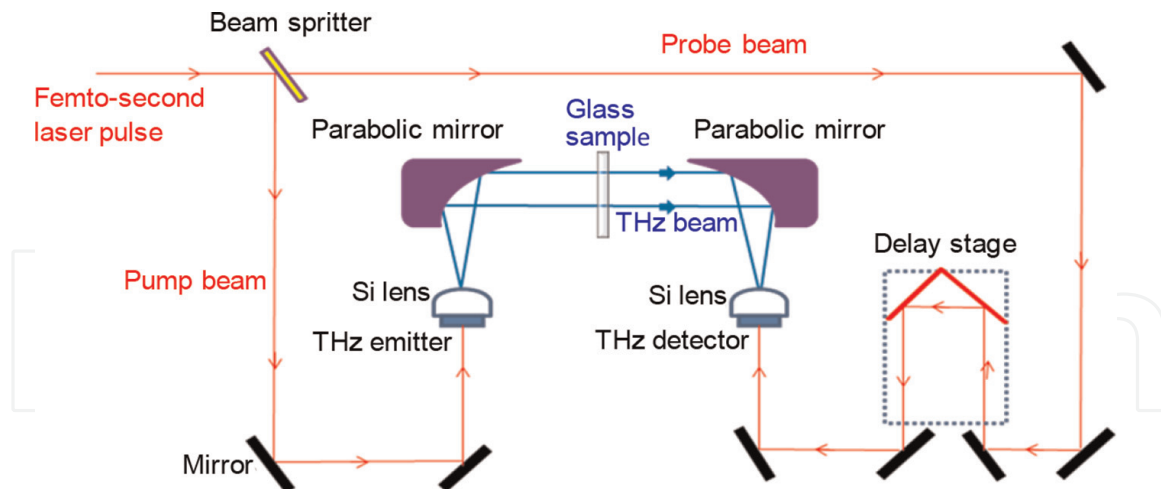


Figure 1.
Schematic diagram of transmission-type photoconductive-antenna-based THz-TDS setup used in this study.

previous work [7, 26]. Briefly, the ultrafast laser used was a Ti:sapphire femto-second laser (Spectra Physics, Tsunami) that routinely generated ~ 60 fs pulses with an average power of 380 mW at 82 MHz. A dipole-type photoconductive antenna (PCA) fabricated on low-temperature molecular-beam-epitaxy-grown GaAs (LT-GaAs) was biased by a periodic step-function-type signals and was excited by the ultrafast laser pulses to generate THz pulses. The generated THz wave was collected using a high-resistivity Si lens and was collimated by gold-coated parabolic mirror into a highly directional beam. After passing through the glass sample, the THz pulse beam was focused onto an identical LT-GaAs PCA as the detector using an identical combination of parabolic mirror and Si lens, as shown in **Figure 1**. The electric field of the transmitted THz pulse induces a voltage across the detector antenna and is mapped by photoconductively shorting the gap. When the detector was gated by a delayed probe laser pulse, a current proportional to the instantaneous field strength of the incident THz pulse can thus be measured using the lock-in technique. The time delay between the pump and probe laser pulse is mechanically scanned by moving a retroreflector with a computer-controlled motor stage. The amplitude and phase of the THz wave were obtained by changing the time delay using this setup. The THz-TDS system was enclosed in a N_2 -purged box with a relative humidity of $\sim 4\%$ to minimize THz power absorption due to residual water vapor in the THz beam path. The glass samples with diameter of ~ 10 mm and thickness of ~ 1.6 mm were polished on both sides. The samples were attached to a sample holder that has an optical aperture ~ 8 mm in diameter. An identical clear aperture was used as a reference.

Typical characteristics of the emitted THz wave in this THz-TDS system are shown in **Figure 2**: (a) displays the measured electric field intensity in time domain and (b) shows the frequency spectrum of THz power, which has been retrieved using the fast Fourier transformation (FFT). The effect of nitrogen purge is obvious for minimizing the water absorption. As shown in the spectrum, the dynamic range of the THz-TDS system is ~ 45 dB at 0.5 THz, and the S/N ratio is maintained in the range of 100–1000 across the band from 0.2 to 1.6 THz.

Figure 3a shows the electric field temporal traces of the transmitted THz wave with and without the glass sample, and **Figure 3b** shows the frequency dependence of the THz phase shift estimated with respect to the reference phase angle (without glass sample). Since the phase shift occasionally showed irregular behavior at high frequency (>0.8 THz, refer to **Figure 3b**) and correspondingly worse S/N ratio, we have

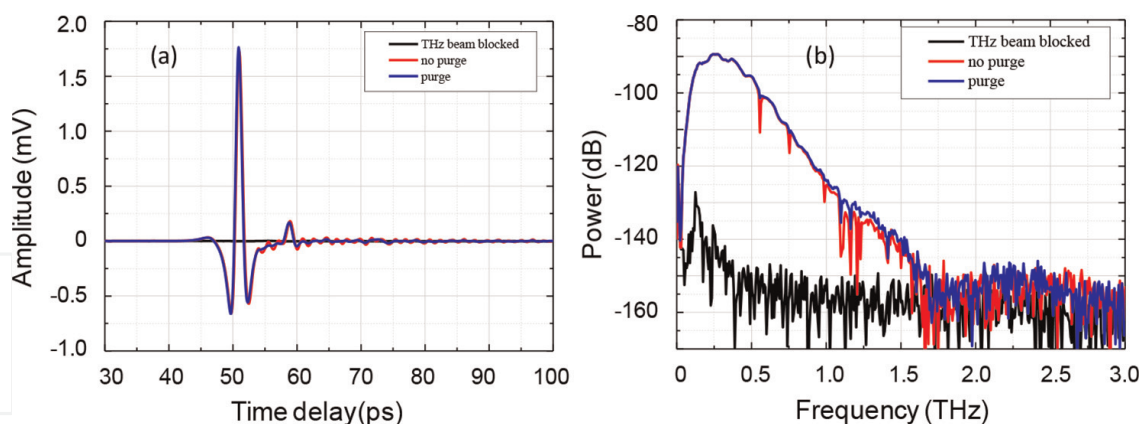


Figure 2. Measured data of (a) time-domain trace of electric field intensity of emitted THz wave and (b) frequency spectrum of emitted THz power as obtained by FFT.

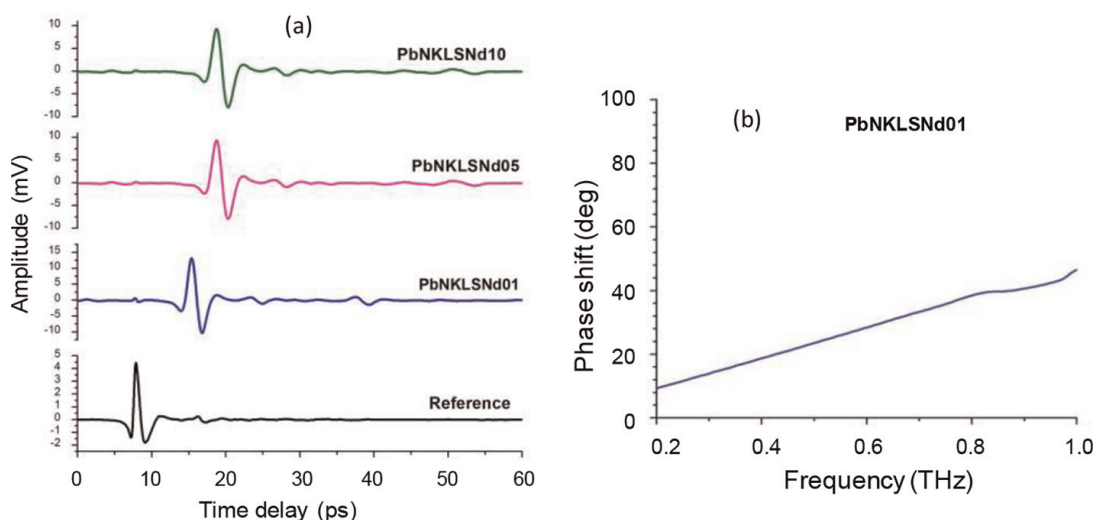


Figure 3. Measured transmission signals for a representative glass sample (PbNKLSNd glasses). (a) Time domain electric field intensity signals of THz waves transmitted through glass samples and air (reference). (b) THz frequency dependence of phase shift caused by transmission through glass sample.

restricted our measurement frequency range between 0.2 and 0.8 THz for the accuracy.

The THz absorption coefficient $\alpha(\nu)$ and refractive index $n(\nu)$ of the glass samples at the frequency ν are determined by using the following equations [12, 26–28];

$$\alpha(\nu) = \frac{2}{d} \ln \left(\left| \frac{E_{ref}(\nu)}{E_{sam}(\nu)} \right| \frac{[n(\nu) + 1]^2}{4n(\nu)} \right) \quad (1)$$

$$n(\nu) = 1 + \frac{c}{2\pi\nu d} (\varphi_{sam}(\nu) - \varphi_{ref}(\nu)) \quad (2)$$

where $E(\nu)$ and $\phi(\nu)$ are the amplitude and phase of the THz field transmitted through the glass sample (suffix: sam) and the reference medium (air in this case, suffix: ref); c is the speed of light, and d is the thickness of glass sample. The second term inside the natural logarithm in the right hand of Eq. (1) is a Fresnel reflection correction factor, for which the effect of extinction coefficient is neglected because of its insignificant effects in the present measurement frequency range (0.2–0.8 THz).

Refractive indices in the transparent range of optical frequencies were evaluated from the normal incidence reflectivity measurement using Fourier transform infrared (FTIR) spectroscopy (Bruker VERTEX v70) by applying the following simplified equation [24, 29]:

$$n_{opt} = \left(1 + r^{1/2}\right) / \left(1 - r^{1/2}\right), \quad (3)$$

where r is the optical reflectivity. The effect of internal multiple reflection within the sample bulk [29] may influence the reflectivity value in the highly transparent wavelength region, but this effect was confirmed to be negligible in our case, supporting the use of simplified equation as shown above [30].

2.2 Glass sample preparation and data acquisition

The OFS glasses were prepared by the melt-quenching technique [19–21, 23] with two series of chemical compositions; one is ZNbKLSNd glass: $(20 - x)\text{ZnF}_2 + 20\text{Nb}_2\text{O}_5 + 20\text{K}_2\text{CO}_3 + 10\text{LiF} + 30\text{SiO}_2 + x\text{Nd}_2\text{O}_3$, and the other is PbNKLSNd glass: $(20-x)\text{PbF}_2 + 5\text{Na}_2\text{O} + 20\text{K}_2\text{CO}_3 + 10\text{LiF} + 45\text{SiO}_2 + x\text{Nd}_2\text{O}_3$, where $x = 1, 5, \text{ and } 10$ mol%. The compositions were designed by referring to our prior works on OFS glasses including ZnF_2 [19] and PbF_2 [21]. Different x values were adopted to check the relative effects of the fluorine and modifier (Nd) contents. Batch composition for each glass with ~ 15 g weight was thoroughly crushed in an agate mortar and its homogeneous mixture was transferred into a platinum crucible and heated at 1250°C for 3 hours in an electric furnace under ambient atmosphere. The melt was then poured onto a preheated brass mold and annealed at 400°C for 10 hrs to remove thermal strains. The glasses were slowly cooled down to room temperature and polished and formed into disks with the thickness of ~ 1.6 mm for the THz and optical measurements. In order to discuss the dielectric properties and their physical mechanisms, data of several of other multi-component glasses, in particular, several commercial silicate oxide glasses have been collected from the literature. Compositions and basic physical parameters including the molecular weight M , density ρ , and molecular volume V_m of glasses used are summarized in **Table 1**. For OFS glasses, the value of ρ was measured by the Archimedes method. The formula weights of glasses were evaluated using nominal atomic compositions.

Glass	Composition	M (g/mol)	ρ (g/cm ³)	V_m (cm ³ /mol)	Ref	
ZNbKLSNd x	$(20-x)\text{ZnF}_2 + 20\text{Nb}_2\text{O}_5 + 20\text{K}_2\text{CO}_3 + 10\text{LiF} + 30\text{SiO}_2 + x\text{Nd}_2\text{O}_3$	$x = 1$	124	3.65	34.0	[23]
		$x = 5$	133	3.66	36.3	
		$x = 10$	145	3.54	41.0	
PbNKLSNd x	$(20-x)\text{PbF}_2 + 5\text{Na}_2\text{O} + 20\text{K}_2\text{CO}_3 + 10\text{LiF} + 45\text{SiO}_2 + x\text{Nd}_2\text{O}_3$	$x = 1$	110	3.72	29.7	[23]
		$x = 5$	114	3.78	30.2	
		$x = 10$	119	3.62	32.8	
Silica	SiO_2	60	2.20	27.3	[12, 23]	
Pyrex	$80.6\text{SiO}_2 + 12.6\text{B}_2\text{O}_3 + 4.2\text{Na}_2\text{O} + 2.2\text{Al}_2\text{O}_3 + 0.04\text{Fe}_2\text{O}_3 + 0.1\text{CaO} + 0.05\text{MgO} + 0.1\text{Cl}$	62	2.23	27.8	[12, 23]	

Glass	Composition	M (g/mol)	ρ (g/cm ³)	V_m (cm ³ /mol)	Ref
BK7	68.9SiO ₂ + 10.1B ₂ O ₃ + 8.8Na ₂ O + 8.4K ₂ O + 2.8BaO + 1.0As ₂ O ₃	65	2.51	26	[12, 23]
SK10	30.6SiO ₂ + 11.7B ₂ O ₃ + 5.0Al ₂ O ₃ + 0.1Na ₂ O + 48.2BaO + 2.0ZnO + 0.7PbO + 0.8Sb ₂ O ₃ + 0.9As ₂ O ₃	112	3.64	30.8	[12, 23]
SF10	35.3SiO ₂ + 2.0Na ₂ O + 2.5K ₂ O + 55.7PbO + 4.0TiO ₂ + 0.5As ₂ O ₃	153	4.28	35.8	[12, 23]
SF6	27.7SiO ₂ + 0.5Na ₂ O + 1.0K ₂ O + 70.5PbO + 0.3As ₂ O ₃	177	5.18	34.2	[12, 23]
S1	La ₂₀ Ga ₂₀ S ₆₀	61	4.27	14.3	[16]
S2	La ₁₆ Ga ₂₄ S ₆₀	58	4.48	13.0	[16]
S3	La ₁₂ Ga ₂₈ S ₆₀	56	4.11	13.6	[16]
S4	La ₁₂ Ga ₂₈ S ₄₈ Se ₁₂	61	3.99	15.3	[16]
S5	La ₁₂ Ga ₂₈ S ₃₉ Se ₂₁	65	4.21	15.4	[16]
S6	Ge ₃₃ As ₁₂ Se ₅₅	76	4.66	16.3	[16]
S7	Ge ₂₈ Sb ₁₂ Se ₆₀	82	4.41	18.6	[16]

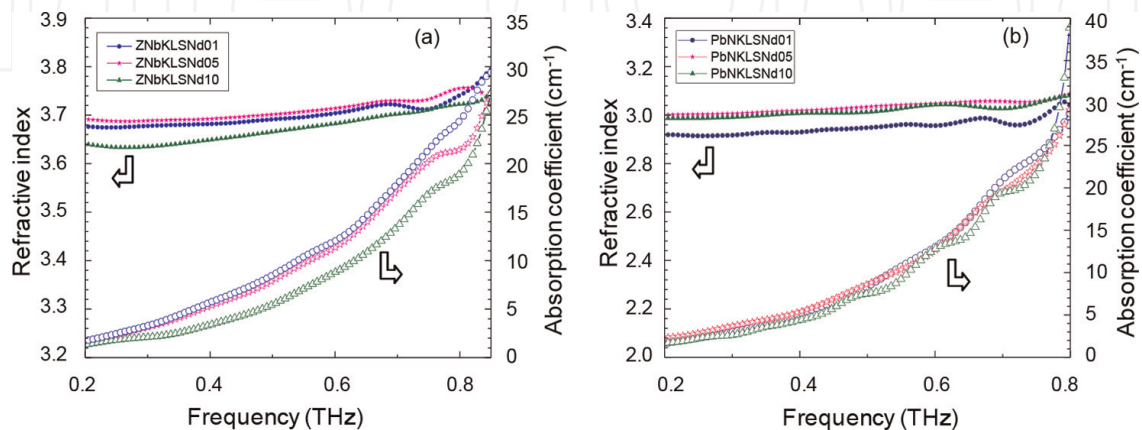
Table 1.

Compositions and basic properties of multi-component glasses (reproduced from ref. [23] with the permission of AIP publishing).

3. Results and discussion

3.1 THz refractive index and absorption coefficient dependences on frequency

Figure 4 shows the absorption coefficients, $\alpha(\nu)$, and the refractive indices, $n(\nu)$ of the OFS glasses as a function of the frequency in the frequency range from 0.2 to 0.8 THz. As shown in **Figure 4**, the refractive index increases gradually and the absorption coefficient increases a little more steeply with the increase of frequency in both OFS glasses. General behaviors of frequency dependent refractive index and absorption coefficient as noticed in our results are consistent with prior reports on

**Figure 4.**

Refractive index and absorption coefficient dependences on THz frequency for (a) ZNbKLSNd and (b) PbNKLSNd glasses with different compositions. (reproduced from ref. [23] with the permission of AIP Publishing).

oxide and chalcogenide glasses in the sub-THz frequency band [12–16]. Although weak oscillatory behaviors are observed at higher frequency regions in some samples possibly due to residual reflection/scattering related effects in the system, this is not too severe to affect the evaluations of basic dielectric parameters. The refractive indices measured in those OFS glasses are higher than in most of the silicate glasses. In particular, ZNbKLSNd glasses exhibit refractive indices as high as 3.70 at 0.5 THz, which is the highest among various silicate glasses so far reported and is close to those of La^{3+} : chalcogenide glasses as reported in Ref. [16]. Another important finding in this result is that the OFS glasses exhibit absorption coefficients significantly lower than those of other glasses known as high-refractive index glasses [12].

A comprehensive physical model of far infrared absorption in solids was discussed for various amorphous materials by Strom et al. [31, 32], in which disorder-induced charge fluctuations in the material structure cause the coupling of THz radiation into atomic vibration modes. This model has been applied recently to interpret the THz absorption characteristics in silicate and chalcogenide glasses [12, 16]. In this model, the product of $n(\nu)$ and $\alpha(\nu)$ is shown to follow a power-law relationship as expressed by [13, 14, 16]:

$$n(\nu)\alpha(\nu) = K(h\nu)^\beta, \quad (4)$$

where K and β are material-dependent parameters of each glass and h is the Planck's constant. We have analyzed the present OFS glasses on the basis of this relationship. **Figure 5** shows the product $n\alpha$ plotted as a function of the THz frequency for ZNbKLSNd and PbNKLSNd glasses. The $n\alpha$ versus frequency behaviors are in fairly good agreement with the slope of 2 as indicated by dashed lines drawn in the figures. The absorption parameter K has therefore been determined for $\beta = 2$ in our analysis on the present OFS glasses. This is consistent with previous data reported for a number of amorphous materials [31, 32], including silicate [12] and chalcogenide [16] glasses, which supports the disorder-induced-charge fluctuation model for interpreting the sub-THz absorption characteristics in a wide variety of glasses. The value of K is associated with the magnitude of incoherent (not maintaining the local charge neutrality) atomic-charge fluctuation induced by structural disorders [13]. The

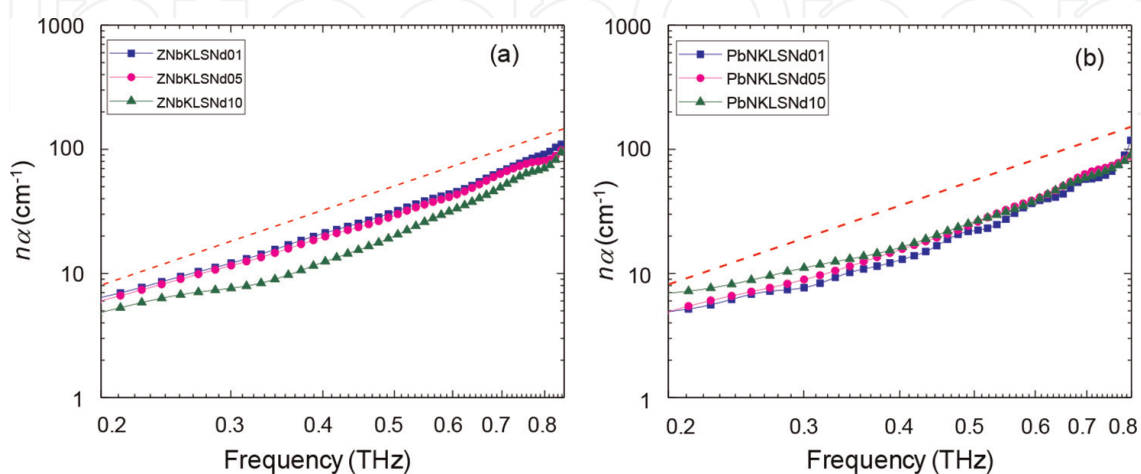


Figure 5. Dependences of refractive index absorption coefficient product on THz frequency for (a) ZNbKLSNd and (b) PbNKLSNd glasses with different compositions. The dotted line is a guide for eye with a slope of 2.0. (reproduced from ref. [23] with the permission of AIP Publishing).

value of β seems to be variable over a wide range ($2 \sim 3.4$ [16, 33]) depending on the alkali modifier contents in oxide glasses [33] and the coordination number in chalcogenide glasses [16]. More detailed interpretation is subject to further study.

3.2 Absorption and refractive index properties in different glasses and their physical origins

The correlation between the THz absorption parameter, K , and refractive index, n , evaluated at 0.5 THz is shown in **Figure 6** for the present OFS glasses and selected other glasses. Glass compositions corresponding to all data points in the figure can be found in [23]. Taking into consideration that the refractive indices of OFS glasses show only small changes in the measured THz frequency range, the K parameter is nearly in proportion to the absorption coefficient according to Eq. (4). The larger K implies larger absorption loss and hence suggests a glass structure involving more and/or heavier disorders. When alkali oxides such as Na_2O are introduced in the silicate oxide glass network structures, covalent Si-O-Si bonds are broken due to larger electronegativity difference between Na (0.93) and Si (1.90). This results in the introduction of local disorders in the glass structure and generates a number of non-bridging oxygens, leading to the increase of the absorption parameter as well as the refractive index [13]. Naftaly et al. [12] showed that K is proportional to the fourth power of the refractive index in a series of commercial multi-component silicate oxide glasses (except for silica), data of which are also shown in **Figure 6**. A trend of the THz absorption coefficient increasing with the THz refractive index is found in most of high-refractive index glasses. Such phenomena can be understood by considering the charge fluctuations that are generated due to the structural disorder when the glass structure is modified. Generation of such atomic charge fluctuations could be enhanced particularly in multi-component glasses such as OFS glasses. As is displayed in **Figure 6**, however, the present OFS glasses show high refractive indices yet maintaining very low absorption coefficients regardless of that their glass

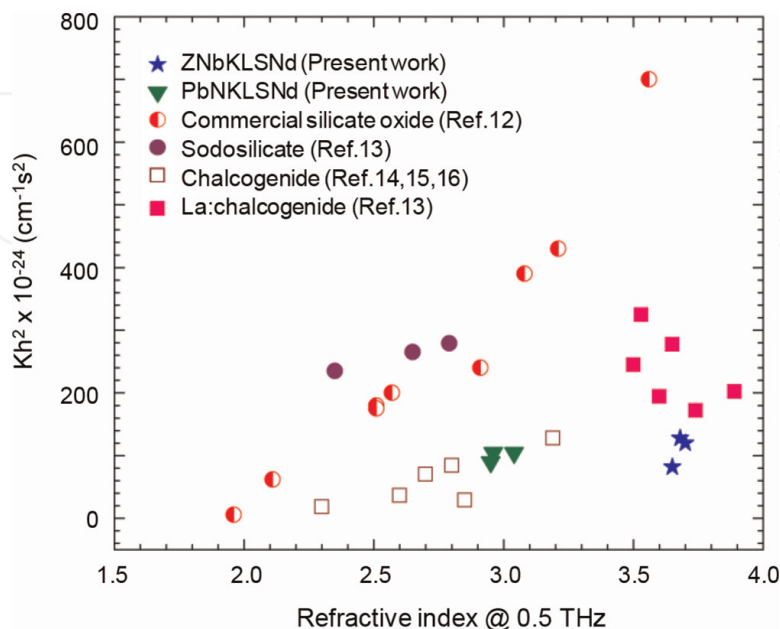


Figure 6. Relationship between the absorption parameter and refractive index determined at 0.5 THz for a variety of multi-component glasses. (reproduced from ref. [23] with the permission of AIP Publishing).

compositions involve appreciable amounts of alkali ions (Na, K) and large atomic weight metal (Nd, Nb) oxides, which would have caused the increase of absorption losses as noticed in most of fluorine-free oxide glasses. Although some more THz-TDS based studies on silicate, germanate, tellurite oxide, and fluoride multi-component glasses have been reported very recently by Pacewicz et al. [33], the highest refractive index and lowest absorption of the present OFS glasses are still valid.

For understanding those properties of OFS glasses, it should be noticed that our OFS glasses incorporate appreciable amounts of fluorides, e.g., ZnF_2 , LiF , and PbF_2 . In many of oxide-based glasses, fluorine is known to restrict the formation of glass network due to its extremely high electronegativity (Pauling: 3.98) [34]. The atomic polarizability (1.04 \AA^3) of fluorine is much lower than that of oxygen (3.88 \AA^3) [35], and this is considered to help reduce the refractive indices of OFS glasses. On the other hand, when the glass network involves structural disorders and strains, the incorporation of fluorine can lead to their relaxation. It was found by Hosono et al. [36] that the introduction of a very small amount ($>1 \text{ mol\%}$) of fluorine into silica results in a significant enhancement of the hardness against ultraviolet radiation. According to their interpretation, the strong F-Si couplings cause the reconstruction of strained three-/four-membered Si-O-Si rings, making the network bonds more open and eventually relaxing physical disorders in the glass structure. It has also been reported that the fluorine substitutes randomly into the oxygen sites [37], and this works favorably to give rise to a uniform structural relaxation. Very low absorption characteristics as found in the present OFS glasses support that the charge fluctuation is considerably prevented in the glass structure owing to the structural relaxation effect of fluorine.

As shown in **Figure 4**, the dependence of the THz absorption coefficient of OFS glasses on the x value is weak. Dependence of the refractive index on x is even weaker. This would suggest that significantly low absorption properties of OFS glasses is predominantly determined by the basic composition of the present OFS glasses, which contain at least 10 mol% of fluorine, rather than by the incorporation of rare earth (Nd) modifier. This is consistent with prior works in which the structural relaxation is observed on the fluorine addition as low as 1 mol% in silica [36, 38]. It can be concluded that the structural relaxation effect of fluorine is primarily responsible for the significantly low absorption loss properties of the present OFS glass systems.

3.3 Dielectric properties and polarizabilities

In order to compare dielectric properties of the present OFS glasses with those of other glasses, we analyze the data by using the Clausius-Mossotti equation [12, 23, 35]. The dielectric constant in the optical frequency range, ϵ_{opt} , is determined by the polarizability of electrons associated with constituent molecules in the glass. On the other hand, the dielectric constant in the sub-THz frequency range, ϵ_{THz} , is determined by the total polarizability including contributions of both the fast response electrons (P_e) and the slow response ions (P_i) involved in the glass material. Both of the dielectric constants, ϵ_{opt} and ϵ_{THz} , are correlated with the molar electronic polarizability, P_e , molar ionic polarizability, P_i , and molar total polarizability, $P_{\text{tot}} = P_e + P_i$, as expressed by the following formula:

$$\frac{\epsilon_{\text{opt}} - 1}{\epsilon_{\text{opt}} + 2} V_m = \frac{4\pi}{3} N_A P_e = R_m^e, \quad (5)$$

$$\frac{\varepsilon_{\text{THz}} - 1}{\varepsilon_{\text{THz}} + 2} V_m = \frac{4\pi}{3} N_A (P_e + P_i) = R_m^{\text{tot}} = R_m^e (1 + a), \quad (6)$$

where V_m is the molar volume which is defined by M/ρ using the density ρ and molecular weight M , R_m^e is the molar electronic refraction, R_m^{tot} is the molar total refraction including both electronic and ionic contributions, a is defined as the ratio P_i/P_e , and N_A is the Avogadro number ($6.023 \times 10^{23} \text{ mol}^{-1}$). Considering that the extinction coefficient ($k = \alpha c / (4\pi\nu)$) is negligible in comparison with the refractive index in the sub-THz region in the present glasses, the THz dielectric constant is obtained from $\varepsilon_{\text{THz}} = n_{\text{THz}}^2$. Similarly the optical dielectric constant is obtained from $\varepsilon_{\text{opt}} = n_{\text{opt}}^2$. By using Eqs. (5) and (6), the polarizabilities can be evaluated from the measured refractive indices in each frequency range. The THz refractive indices have been determined at a fixed frequency of 0.5 THz for all glasses in this study. The optical refractive indices of OFS glasses have been determined at the wavelength of 1500 nm from the measured optical reflectivity spectra using Eq. (3). For other commercial glasses, the refractive indices determined at 589 nm [12] have been used. The resultant values of polarizabilities P_e , P_i and P_{tot} , and $a = P_i/P_e$ are summarized in **Table 2**.

Glass	n_{THz}	n_{opt}	P_{tot} (\AA^3)	P_e (\AA^3)	P_i (\AA^3)	$a =$ P_i/P_e	ε_{THz} - ε_{opt}	λ_0 (μm)	g ($10^{10} \text{ cm}/$ mol)	Ref.
ZNbKLSNd01	3.68	1.81	10.9	5.82	5.05	0.868	10.27	74.57	6.247	[24]
ZNbKLSNd05	3.70	1.79	11.7	5.99	5.67	0.947	10.49	78.89	6.066	[24]
ZNbKLSNd10	3.65	1.80	12.6	6.83	5.80	0.850	10.08	98.72	4.186	[24]
PbNKLSNd01	2.95	1.57	8.47	3.79	4.68	1.24	6.24	126.5	1.279	[24]
PbNKLSNd05	3.04	1.63	8.77	4.19	4.58	1.10	6.58	112.6	1.510	[24]
PbNKLSNd10	2.96	1.53	9.38	3.94	5.44	1.38	6.42	115.5	1.617	[24]
Silica	1.96	1.46	5.26	2.91	2.35	0.810	1.71			[12, 24]
Pyrex	2.11	1.47	5.90	3.02	2.88	0.950	2.27			[12, 24]
BK7	2.51	1.52	6.60	3.09	3.51	1.15	3.99	80.84	1.586	[12, 24]
SK10	2.91	1.62	8.71	4.29	4.42	1.03	5.85	126.7	1.082	[12, 24]
SF10	3.21	1.73	10.7	5.66	5.07	0.900	7.31	138.7	1.305	[12, 24]
SF6	3.56	1.81	10.8	5.86	4.93	0.840	9.40	132.5	1.762	[12, 24]
S1	3.89	2.37	4.60	3.38	1.22	0.361	9.52	108.8	1.110	[16, 24]
S2	3.74	2.38	4.20	3.07	1.13	0.368	8.32	110.4	0.953	[16, 24]
S3	3.60	2.37	4.30	3.22	1.08	0.335	7.34	95.68	1.064	[16, 24]
S4	3.50	2.31	4.80	3.53	1.27	0.360	6.91	91.41	1.343	[16, 24]
S5	3.65	2.37	4.90	3.65	1.25	0.343	7.71	93.09	1.343	[16, 24]
S6	2.85	2.73	4.60	4.36	0.24	0.055	0.67	139.4	0.303	[16, 24]
S7	3.19	2.60	5.60	4.79	0.81	0.169	3.42	139.7	0.052	[16, 24]

Table 2.

Material, THz, and optical parameters determined for a variety of glasses (reproduced from ref. [23] with the permission of AIP publishing).

By using this ratio a , the electronic molar refraction R_m^e and the molar volume V_m , the optical refractive index (n_{opt}) and THz refractive index (n_{THz}) can be expressed in the following forms:

$$n_{opt} = \sqrt{\frac{1 + 2R_m^e/V_m}{1 - R_m^e/V_m}}, \quad (7)$$

$$n_{THz} = \sqrt{\frac{1 + 2R_m^e(1 + a)/V_m}{1 - R_m^e(1 + a)/V_m}}. \quad (8)$$

Figure 7 shows the relationships between the THz refractive index and optical refractive index for various silicate oxide glasses including OFS glasses and La:chalcogenide glasses. Two curves indicated in the figure have been obtained from Eqs. (7) and (8) using R_m^e/V_m as a variable parameter for fixed values of a ; $a = 0.95$ and $a = 0.35$ have been assumed for silicate oxides and La:chalcogenides, respectively, in **Figure 7**. As shown in this figure, two different glass groups are distinguished by the polarizability ratio a . Small shifts of the measured data from the calculated curve are due to the discrepancy of the real value of a from the fixed value used for calculation, for example, $a = 0.85\text{--}0.95$ for ZNbKLSNd glasses and $a = 1.10\text{--}1.38$ for PbNKLSNd glasses, as can be confirmed in **Table 2**. A similar n_{opt} vs. n_{THz} relationship is found for La:chalcogenide glass group. On the basis of the present result, the polarizability ratio a can be a useful parameter to characterize the chemical composition/structure of glass materials at least within the same glass family such as silicate oxide glasses, in which the common oxygen ion O^{2-} is responsible to control the dielectric property.

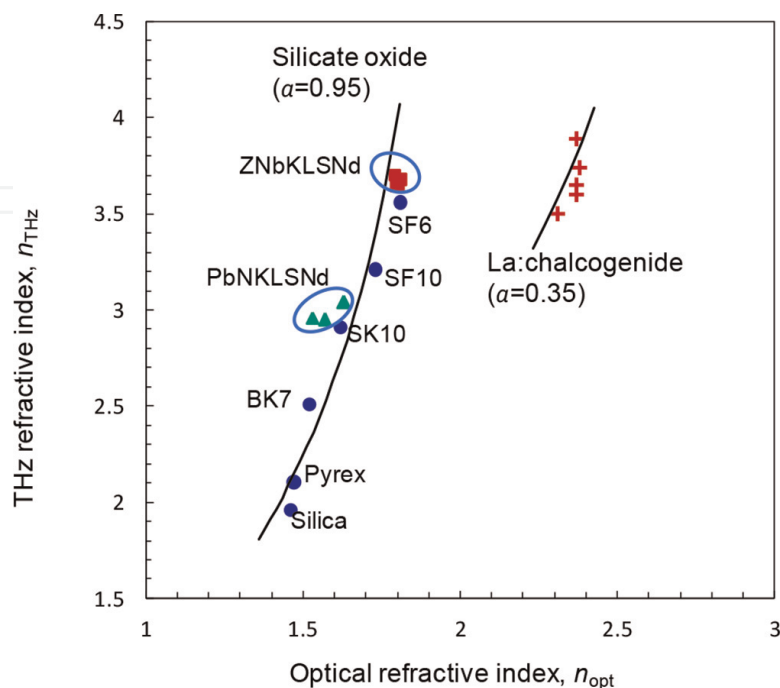


Figure 7. Relationship of THz refractive index as a function of optical refractive index for various glasses. Curves shown have been calculated with representative values of $a = P_i/P_e$. (ref. [24]).

3.4 Ionic contribution to dielectric properties of silicate oxide glasses

We have so far seen that the electronic and ionic contributions to the dielectric and absorption properties of glasses are interpreted by a unified relationship for all silicate oxide glasses. In the following, we focus on the contribution of the ionic vibrations to the dielectric properties of glasses by using a simplified dielectric model [24] and discuss their relation with the physical properties of glasses. The dielectric constant (ϵ) at a given frequency (ν) in the THz and far-infrared (FIR) region, ϵ_ν , can be represented by the classical single harmonic oscillator model (Lorentz model), which describes the displacement of a pair of anion and cation, as is expressed by [39, 40]:

$$\epsilon_\nu = \epsilon_\infty + \frac{4\pi N e^2}{\mu} \frac{f}{\nu_0^2 - \nu^2 - i\gamma\nu}, \quad (9)$$

where ϵ_∞ is the dielectric constant at the infinite frequency ($\nu = \infty$), N is the number of unit cells involving ion pairs per unit volume ($= N_A/V_m$), e is the electronic charge, μ is the reduced mass of ions given by $1/\mu = 1/m_+ + 1/m_-$, where m_+ and m_- are the masses of anion and cation, ν_0 is the characteristic resonance frequency of the oscillator, f is the oscillator strength, and γ is the damping factor for displacement. Here, single charge anion-cation pairs are assumed for simplicity; that is, a single parameter ν_0 will represent the oscillator resonance frequency and eventually control the THz dielectric characteristics of the glass. Also when the frequency range of our interest is far from the resonance frequency (as will be confirmed later), the damping factor can be neglected in Eq. (9). For the convenience of analysis, Eq. (9) is rewritten to express the dielectric constant, ϵ_ν , as a function of the wavelength $\lambda (= c/\nu)$, as shown by the following form (Drude-Voigt relation [41, 42]):

$$\frac{1}{\epsilon_\nu - \epsilon_\infty} = \frac{\pi c^2 \mu V_m}{N_A e^2 f} \left(\frac{1}{\lambda_0^2} - \frac{1}{\lambda^2} \right), \quad (10)$$

where $N = N_A/V_m$ and the oscillator resonance wavelength λ_0 have been used. When we define a material dependent amplitude factor g as:

$$g = \frac{N_A e^2 f}{\pi c^2 \mu}, \quad (11)$$

Eq. (10) can be written as:

$$\frac{1}{\epsilon_\nu - \epsilon_\infty} = \frac{V_m}{g} \left(\frac{1}{\lambda_0^2} - \frac{1}{\lambda^2} \right). \quad (12)$$

This indicates that a plot of $1/(\epsilon_\nu - \epsilon_\infty)$ as a function of $1/\lambda^2$ gives a straight line, and its slope gives the value of g through $g = V_m / [\text{slope}]$. Considering the y -intercept $1/(\epsilon_\nu - \epsilon_\infty)$ of this plot for $\lambda \rightarrow \infty (\nu \rightarrow 0)$, Eq. (12) leads to the following relation:

$$\epsilon_{\nu=0} - \epsilon_\infty = \frac{g \lambda_0^2}{V_m}. \quad (13)$$

Therefore, [slope]/[y-intercept] provides the value of λ_0^2 for each of the glass material.

In the present analysis, the values of ϵ_∞ have been determined from the refractive indices measured at the optical wavelength by using the relation $\epsilon_\infty = \epsilon_{\text{opt}} = n_{\text{opt}}^2$. For $\epsilon_{\nu=0}$, we have used the value of $\epsilon(\nu = 0.2 \text{ THz}) = \epsilon_{\text{THz}} = n_{\text{THz}}^2$ since ϵ_ν virtually saturates at 0.2 THz (**Figure 4**). In **Figure 8a**, $1/(\epsilon_\nu - \epsilon_\infty)$ is plotted as a function of $1/\lambda^2$ for ZNbKLSNd x ($x = 1, 5, 10$) and PbNKLSNd x ($x = 1, 5, 10$) glasses, and all the plots show reasonable linear dependences. From these plots, the g factor and λ_0 values have been determined, as listed in **Table 2**. The same procedure has been carried out for other silicate oxide glasses by using the data reported by Naftaly et al. [12], and the resultant plots are shown in **Figure 8b** for selected multi-component silicate oxide glasses. Some of the THz-TDS data have shown only weak frequency dependences (e.g., silica and Pyrex [12]) and those data have been omitted for the accuracy in the present analysis. The values of g and λ_0 determined for all glasses including La:chalcogenide glasses are included in **Table 2**.

Results shown in **Figure 8** indicate that THz dielectric constant characteristics of all the glasses studied here can be interpreted by a simplified form of single oscillator model. Eq. (12) indicates that the dielectric constant difference ($\epsilon_\nu - \epsilon_\infty$), corresponding to the ionic vibration contribution at the frequency ν , is governed by the values of V_m , g and λ_0 , which are all specific to the glass material under test. In order to observe the ionic vibration contributions to the dielectric constants in different glasses, we have plotted in **Figure 9** the dielectric constant difference $\epsilon_{\text{THz}} - \epsilon_{\text{opt}}$ as a function of $g\lambda_0^2/V_m$. We adopt the value of $\epsilon(\nu = 0.2 \text{ THz})$ as ϵ_{THz} for estimating $\epsilon_{\text{THz}} - \epsilon_{\text{opt}}$, and all other parameters are taken from the experimental data already described. **Figure 9** clearly shows a linear relationship regardless of the difference of glass materials (including La:chalcogenide glasses: plots not shown). This result confirms the wide applicability of the single oscillator model for assessing THz dielectric properties in a wide variety of glass materials.

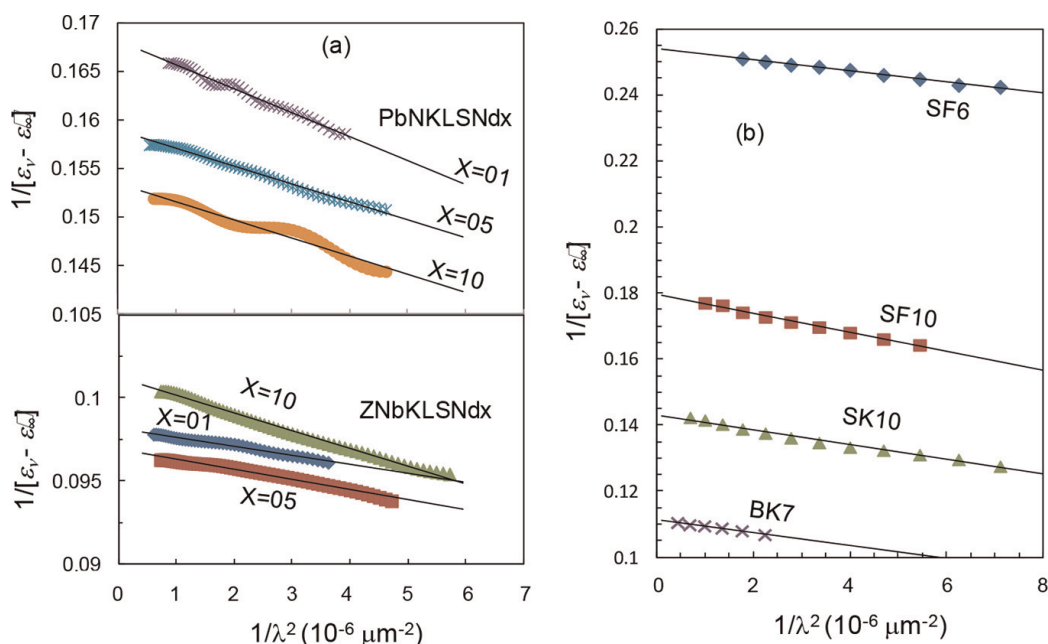


Figure 8. $1/(\epsilon_\nu - \epsilon_\infty)$ versus $1/\lambda^2$ plots for (a) ZNbKLSNd and PbNKLSNd glasses with different compositions and (b) selected multi-component silicate oxide glasses. (ref. [24]).

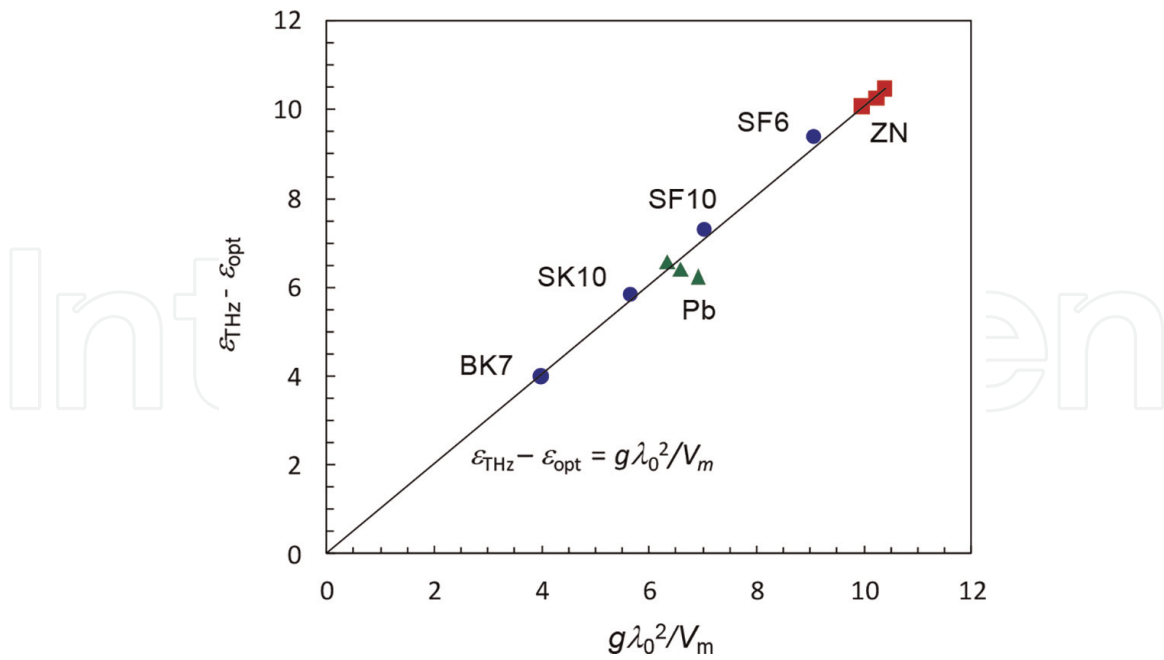


Figure 9. Relationship between $\epsilon_{\text{THz}} - \epsilon_{\text{opt}}$ versus $g\lambda_0^2/V_m$ for selected silicate oxide glasses. Plots show experimental data determined from the single oscillator analysis and the straight line indicates a slope of unity. (ref. [24]).

As we have seen already, OFS glasses possess THz dielectric constants much larger than for most of other glasses, and it is very interesting and important to know the physical origin of such dielectric constant enhancement. For finding out what physical parameter controls the ionic dielectric constant, $\epsilon_{\text{THz}} - \epsilon_{\text{opt}}$ has been plotted as a function of each of the parameters: $1/V_m$, g and λ_0^2 , as is shown in **Figure 10**. Here, $1/V_m$ is regarded as a parameter in proportion to the number of ion pairs in a unit volume. Two other parameters, g and λ_0^2 , are adopted to represent the nature of vibrational oscillator. As **Figure 10a** indicates, the molar volume seems not to influence seriously the dielectric constant difference $\epsilon_{\text{THz}} - \epsilon_{\text{opt}}$. **Figure 10b** and **c** show

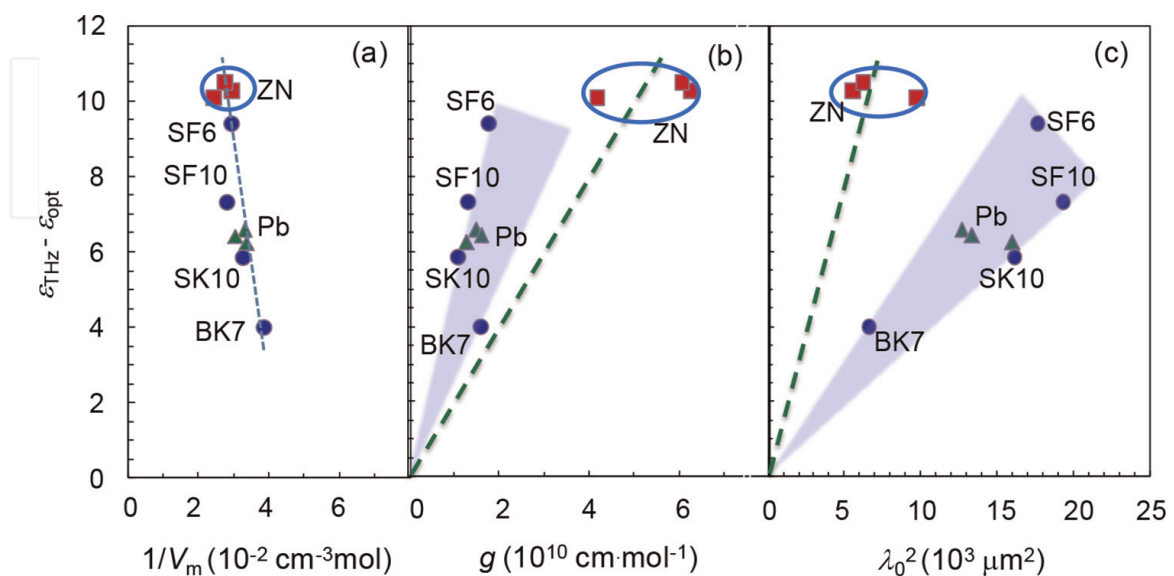


Figure 10. The dielectric constant difference $\epsilon_{\text{THz}} - \epsilon_{\text{opt}}$ as functions of $1/V_m$, g and λ_0^2 for silicate oxide glasses including PbNKLSNd (Pb) and ZNbKLSNd (ZN) glasses. A significant behavior difference is found between ZNbKLSNd glasses and other silicate oxide glasses. (ref. [24]).

general trends, in which the dielectric constant difference increases in proportion to g as well as λ_0^2 , supporting the trend of Eq. (13). Looking at the g and λ_0^2 dependences more closely, it is noticed that there are two distinct groups: ZNbKLSNd glasses, and all other silicate oxide glasses. In ZNbKLSNd glasses, an extremely large dielectric constant enhancement ($\epsilon_{\text{THz}} - \epsilon_{\text{opt}} > 10$) is achieved due to the significantly large value of g (rather than by λ_0^2). In the group of other silicate oxide glasses including PbNKLSNd glasses, the enhancement of the dielectric constant is caused contrastively by the large values of λ_0^2 (rather than by g). Thus, the present analysis based on the single oscillator model has elucidated that the different physical parameters are responsible for the ionic dielectric constant enhancement in different glass groups; the large g plays a principal role in ZNbKLSNd glasses and the large λ_0^2 plays leading roles in other silicate oxide glasses.

3.5 Dielectric property analysis using unified single oscillator model

3.5.1 Single oscillator-based formalism for dielectric property analysis

As we have seen in the previous section, a simplified form of single oscillator model has been found to be useful as a unified model to characterize the THz dielectric constant properties in all the glass groups studied. However, the analysis has assumed the diatomic chain vibration without considering the local field effect. To properly discuss the behavior of electromagnetic waves induced by ionic vibration, the application of phonon polariton formalism with the inclusion of the local field effect is useful [43–47]. In the following, we summarize the basic dielectric function and some useful relations for characterizing dielectric properties by referring to Gresse's approach [47]. In this section, SI unit is used for convenience, but the conversion to CGS unit can be done by replacing the vacuum dielectric constant ϵ_0 by $1/4\pi$.

We assume a single oscillator model based on simple diatomic chain for describing the ionic vibration to determine the dielectric functions of glass materials. An equation of motion which describes the relative displacement of the cation-anion pair \mathbf{u} is written in the following form:

$$\mu\ddot{\mathbf{u}} + \mu\gamma\dot{\mathbf{u}} + D\mathbf{u} = q^* \mathbf{E}_{loc}, \quad (14)$$

where μ is the reduced mass of ions defined by $1/\mu = 1/m_+ + 1/m_-$, where m_+ and m_- are the anion and cation masses, γ is the damping factor for displacement, D is the force constant of the ionic pair, and q^* is the effective charge of ion. \mathbf{E}_{loc} stands for the local electric field involving the microscopic Lorenz field applied to an atom. This local field is correlated with the macroscopic applied field \mathbf{E}_a and polarization \mathbf{P} by the following equation:

$$\mathbf{E}_{loc} = \mathbf{E}_a + \frac{1}{3} \cdot \frac{\mathbf{P}}{\epsilon_0} = \left(\frac{1}{\chi} + \frac{1}{3} \right) \frac{\mathbf{P}}{\epsilon_0}, \quad (15)$$

where a macroscopic relation of the applied field \mathbf{E}_a with the polarization, $\mathbf{P} = \epsilon_0\chi\mathbf{E}_a$, has been used. Here, ϵ_0 and χ are the vacuum dielectric constant and macroscopic electric susceptibility of the material. The total polarization \mathbf{P} consists of the lattice strain (\mathbf{u}) induced dipole moment (\mathbf{P}_{PH}), which is originated from the relative ion core displacement, and the electronic polarization (\mathbf{P}_{VE}), which is caused

by the valence electron displacement with respect to ion core in the local field. This correlation is expressed by:

$$\mathbf{P} = \mathbf{P}_{PH} + \mathbf{P}_{VE} = Nq^* \mathbf{u} + N\varepsilon_0 P_e \mathbf{E}_{loc}, \quad (16)$$

where N is the number of atoms in unit molecule ($N = N_A/V_m$) and P_e is the electronic polarizability of valence electrons surrounding the steady ion core (without lattice strain). The influence of valence electron displacement which is caused by the lattice strain is taken into account through the effective charge q^* of ion pair. Applying the form of harmonic electric field ($\mathbf{E}_a \propto \exp(-i\omega t)$), Eq. (14) can be written as:

$$(\omega^2 + i\omega\gamma - \omega_0^2) \mathbf{u} + \frac{q^*}{\mu} \mathbf{E}_{loc} = 0, \quad (17)$$

where ω_0 is defined as $\omega_0^2 = D/\mu$ by using the force constant D , and ω_0 indicates the intrinsic resonance frequency for the undamped vibration of diatomic chain under zero electric field: $\ddot{\mathbf{u}} + \omega_0^2 \mathbf{u} = 0$.

Eqs. (15)–(17) form a set of homogeneous equations for \mathbf{u} , \mathbf{P} and \mathbf{E}_{loc} (Huang-Szigetti equation [47]). By solving the secular equation for the macroscopic susceptibility χ , the following relation is obtained:

$$\chi = \frac{3(NP_e + \chi_0)}{3 - (NP_e + \chi_0)}. \quad (18)$$

Here, NP_e and χ_0 indicate the microscopic electronic and ionic susceptibilities. The microscopic ionic susceptibility, χ_0 , is induced by the ionic vibration, in which effects of valence electron polarization ($N\varepsilon_0 P_e \mathbf{E}_{loc}$) and the induced local field ($\mathbf{P}/3\varepsilon_0$) are excluded, and is expressed by:

$$\chi_0 = \frac{\omega_p^2}{\omega_0^2} \cdot \frac{\omega_0^2}{\omega_0^2 - \omega^2 - i\omega\gamma}. \quad (19)$$

where ω_p is the ionic vibration resonance frequency which is defined by $\omega_p^2 = \frac{Nq^{*2}}{\varepsilon_0\mu}$. With a slight manipulation of Eq. (18) using the relation of $\varepsilon = 1 + \chi$, it is readily shown that the dielectric constant at the frequency ω , $\varepsilon(\omega)$, can be expressed by the following simple form equivalent to Eq. (9):

$$\varepsilon(\omega) = \varepsilon_\infty + (\varepsilon_s - \varepsilon_\infty) \frac{\omega_T^2}{\omega_T^2 - \omega^2 - i\omega\gamma}, \quad (20)$$

where ε_s and ε_∞ are the values of ε at the frequency $\omega \rightarrow 0$ and $\omega \rightarrow \infty$, respectively, and ω_T is the renormalized resonant frequency which is lowered from ω_0 due to the local field effect as is expressed by:

$$\omega_T^2 = \omega_0^2 - \frac{1}{3 - NP_e} \omega_p^2 = \omega_0^2 - \frac{1}{3} \omega_p^2 \frac{\varepsilon_\infty + 2}{3}. \quad (21)$$

To distinguish the effects of the ionic vibration (\mathbf{P}_{PH}) and valence electron displacement (\mathbf{P}_{VE}) contributions in the determination of the overall polarization, it is necessary to evaluate the microscopic electronic and ionic susceptibility components,

NP_e and $(\omega_p/\omega_0)^2$, respectively (refer to Eqs. (18) and (19)). Since those quantities cannot be directly measured, it would be convenient if they could be monitored by using the measurable physical parameters such as the dielectric constants, ϵ_s and ϵ_∞ , and the renormalized characteristic frequency, ω_T , etc. Interestingly, this is made possible by using the following equations, which are deduced from Eqs. (18)–(21):

$$\epsilon_\infty = \frac{3 + 2NP_e}{3 - NP_e}, \quad (22)$$

$$\epsilon_s = \frac{3 + 2\left((NP_e + (\omega_p/\omega_0)^2)\right)}{3 - \left((NP_e + (\omega_p/\omega_0)^2)\right)}, \quad (23)$$

$$\frac{\omega_T}{\omega_0} = \left(1 - \frac{1}{3 - NP_e} \left(\frac{\omega_p}{\omega_0}\right)^2\right)^{1/2}. \quad (24)$$

It would be noteworthy that we can also deduce from Eqs. (18)–(21) very simple and convenient relations to determine NP_e , ω_p/ω_0 and ω_T/ω_0 and a parameter by using only the steady state values of dielectric constants, ϵ_s and ϵ_∞ , as shown in the following:

$$NP_e = \frac{3(\epsilon_\infty - 1)}{\epsilon_\infty + 2}, \quad (25)$$

$$\frac{\omega_p}{\omega_0} = \left(\frac{9(\epsilon_s - \epsilon_\infty)}{(\epsilon_s + 2)(\epsilon_\infty + 2)}\right)^{1/2}, \quad (26)$$

$$\frac{\omega_T}{\omega_0} = \left(\frac{\epsilon_\infty + 2}{\epsilon_s + 2}\right)^{1/2}, \quad (27)$$

$$a = \frac{P_i}{P_e} = \frac{3(\epsilon_s - \epsilon_\infty)}{(\epsilon_s + 2)(\epsilon_\infty - 1)}. \quad (28)$$

Considering $\epsilon_\infty = \epsilon_{\text{opt}}$ and $\epsilon_s = \epsilon_{\text{THz}}$, all those characteristic parameters are readily determined by only using the dielectric constants obtained in the optical and THz spectroscopic measurements. This feature is particularly advantageous as a unified model for the assessment of physical properties of different glass materials.

3.5.2 Comparison between theory and experiment

We analyze the measured dielectric properties of different glasses by using the relations described above. The renormalized characteristic frequency ω_T corresponds to the characteristic resonance wavelength λ_0 as used in Section 3.4 through $\omega_T = 2\pi c/\lambda_0$. All the characteristic parameters, NP_e , ω_p/ω_0 and ω_T/ω_0 and a , are obtained by using Eqs. (25)–(28) and the result is summarized in **Table 3**.

In **Figure 11**, a set of three-dimensional maps are shown to visualize the behaviors of (a) ϵ_s , (c) ω_T/ω_0 , (e) ϵ_∞ , and (f) a parameter on the planes of NP_e and ω_p/ω_0 . **Figure 11 (b)** and **(d)** show the values of **(b)** ϵ_s and **(d)** ω_T/ω_0 which have been obtained from the experimental data of ϵ_s and ϵ_∞ . As is realized in **Figure 11e** and also in Eq. (22), ϵ_∞ is independent from the ionic contribution and is determined solely by

Glass	ϵ_{THz}	ϵ_{opt}	a	ω_T^2 ($\times 10^2 \text{ THz}^2$)	$\epsilon_s - \epsilon_\infty$	NP_e	ω_p/ω_0	ω_T/ω_0	I_p	Ref
ZNbKLSN01	13.54	3.27	0.868	6.39	10.26	1.294	1.061	0.583	0.465	[25]
ZNbKLSN05	13.69	3.20	0.947	5.71	10.49	1.271	1.075	0.576	0.476	[25]
ZNbKLSN10	13.32	3.24	0.850	3.65	10.08	1.282	1.063	0.585	0.468	[25]
PbNKLSN01	8.70	2.46	1.23	2.22	6.238	0.984	1.084	0.646	0.544	[25]
PbNKLSN05	9.24	2.66	1.09	2.80	6.585	1.067	1.064	0.644	0.515	[25]
PbNKLSN10	8.76	2.34	1.38	2.66	6.421	0.927	1.112	0.635	0.572	[25]
Silica	3.84	2.13	0.808		1.710	0.822	0.799	0.841	0.437	[12, 25]
Pyrex	4.43	2.16	0.954		2.270	0.837	0.874	0.804	0.477	[12, 25]
BK7	6.30	2.31	1.14	5.44	3.990	0.912	1.002	0.721	0.524	[12, 25]
SK10	8.47	2.62	1.03	2.21	5.844	1.053	1.042	0.665	0.508	[12, 25]
SF10	10.30	2.99	0.896	1.85	7.311	1.197	1.035	0.637	0.472	[12, 25]
SF6	12.67	3.28	0.841	2.02	9.398	1.294	1.046	0.600	0.458	[12, 25]

Table 3.

THz and optical dielectric parameters determined for a variety of glasses (ref. [25]).

the polarization due to the valence electron contribution. In contrast, ϵ_s is controlled by both the electron and ion contributions, and it increases rapidly as those contributions become larger, as is displayed in **Figure 11a**. The contours delineated for $NP_e < 3$ and $\omega_p/\omega_0 < 3^{1/2}$ on the base planes in **Figure 11b** and **d** indicate the limits of existence of ϵ_s where the catastrophic collapse of glass phase occurs and the dielectric constant diverges to infinity. In **Figure 11b**, measured data of ϵ_s are displayed for various silicate oxide glasses and also for two La: chalcogenide glasses (S1 and S5 in **Table 2**) [16, 24, 25]. As for OFS glasses, only data for $x = 5$ are shown for avoiding complexity of the figure. The comparison between figures (a) and (b) indicates a good correspondence between the experimental and calculated results for all glasses. More precise comparison has been reported in [25]. Since chalcogenide glasses are known to be highly covalent in comparison with silicate oxide glasses, they appear at locations with higher NP_e and lower ω_p/ω_0 than for silicate oxide glasses.

In **Figure 11c** and **d**, calculated and measured values of ω_T/ω_0 are shown (for OFS glasses, $x = 5$ only) with a different viewing angle for the ease of observing the overall trend. It is clearly seen that as the electronic and ionic contributions increase, the characteristic frequency exhibits a severe softening (lowering) toward the catastrophic boundary where ω_T becomes zero and ϵ_s diverges to infinity. As shown in those figures, the experimental data support the calculated trend. This softening behavior of ω_T/ω_0 corresponds to the diverging increase of the THz dielectric constant, and this feature can be used for detecting the characteristic change of dielectric property. **Figure 11f** shows the behavior of a parameter as evaluated by Eq. (28), which exhibits a non-monotonous variation in contrast to the behaviors of ϵ_s and ϵ_∞ .

Those results suggest that the dielectric parameters in the glasses examined here are influenced primarily by the ionic vibration originated polarization ($(\omega_p/\omega_0)^2$) but precise parameter values are modified by the valence electron polarization effect

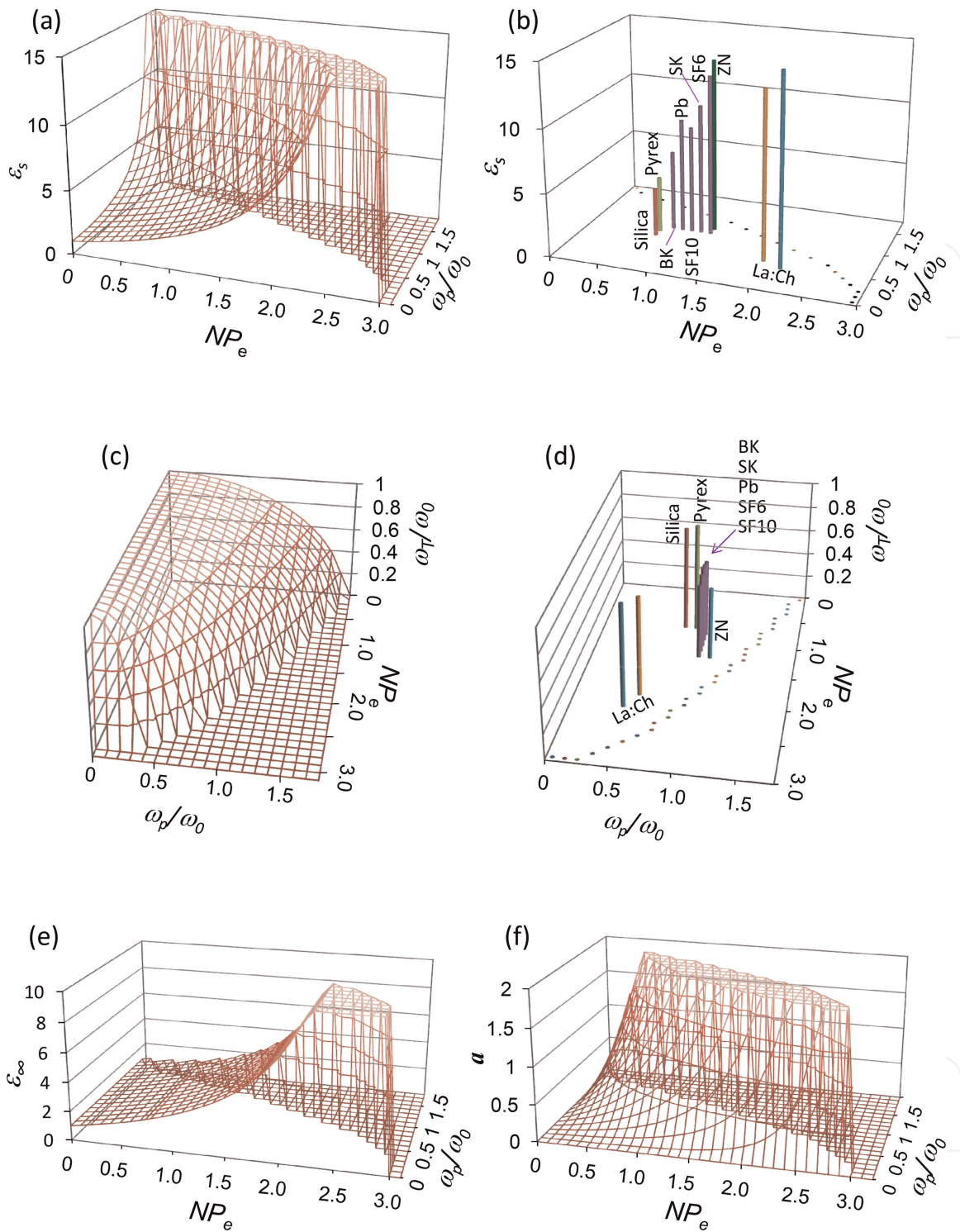


Figure 11. A variety of the dielectric parameters (a), (b): ϵ_s , (c), (d): ω_T/ω_0 , (e): ϵ_∞ , and (f): $a = P_i/P_e$ plotted on the base planes of NP_e and ω_p/ω_0 . Plots in (a), (c), (e), and (f) show the results calculated by using Eqs. (22)–(24), and plots in (b) and (d) show measured ϵ_s and ω_T/ω_0 evaluated from measured ϵ_s and ϵ_∞ values using Eqs. (25)–(28). (ref. [25]).

(NP_e). This explains the reason of data scattering in the ϵ_s versus ϵ_∞ relationship as noticed in **Figure 7**, and accurate values of NP_e and $(\omega_p/\omega_0)^2$ should be taken into account for exact fitting. Precise comparison has confirmed the consistency between the model and experiment, as has been described in Ref. [25]. This indicates that

values of all key parameters necessary for the analysis can be determined simply from Eqs. (25)–(28).

Here, we look at the behavior of a parameter in more detail. As is noticed in **Figure 11f**, the envelope of a parameter variation drawn on the $NP_e - \omega_p/\omega_0$ plane is warped differently when compared with the envelopes of ε_∞ (**Figure 11e**) and ε_s (**Figure 11a**). Actually in **Figure 7**, the a parameter value, which is required for fitting the Clausius-Mossotti curves and measured ε_{opt} and ε_{THz} data, exhibits a fairly complicated behavior (e.g., double-valued ε_{opt} for the same a ; refer to **Table 2**) as already mentioned above. Such a non-monotonous behavior of a is readily understood by taking account of the difference in the envelope warp for a and ε_∞ : when NP_e increases, ε_∞ also increases, whereas a parameter can either increase or decrease depending on the value of ω_p/ω_0 .

We define here the polarization ionicity I_P which is expressed by:

$$I_P = \frac{P_i}{P_e + P_i} = \frac{(\omega_p/\omega_0)^2}{NP_e + (\omega_p/\omega_0)^2} = \frac{3(\varepsilon_s - \varepsilon_\infty)}{(\varepsilon_s - 1)(\varepsilon_\infty + 2)} = \frac{a}{1 + a}, \quad (29)$$

where Eqs. (22)–(28) have been used. The values of I_P evaluated for different glasses are included in **Table 3**. **Figure 12** shows the overview of I_P behavior in the $NP_e - \omega_p/\omega_0 - I_P$ space, in which I_P exhibits monotonous variation and a diverging behavior as seen for the a parameter (**Figure 11f**) is eliminated. Because of this nature, although both parameters, a and I_P , represent essentially the degree of ionicity, I_P is considered to be more useful for characterizing the ionic contribution in the low-frequency dielectric constant of materials. For example, the discussion in Section 3.3 can be rephrased by using I_P instead of $a (= I_P/(1 - I_P))$ so that the ionicity effect is expressed more explicitly.

3.5.3 Assessment of dielectric constant enhancement in OFS glasses

We have shown earlier in **Figure 10** that ZNbKLSNd glass shows appreciably higher g factor and significantly smaller λ_0^2 in comparison with those of most all other silicate oxide glasses. However, g factor in Eq. (9) corresponds to $(\varepsilon_s - \varepsilon_\infty)\omega_T^2$ in Eq. (20) and

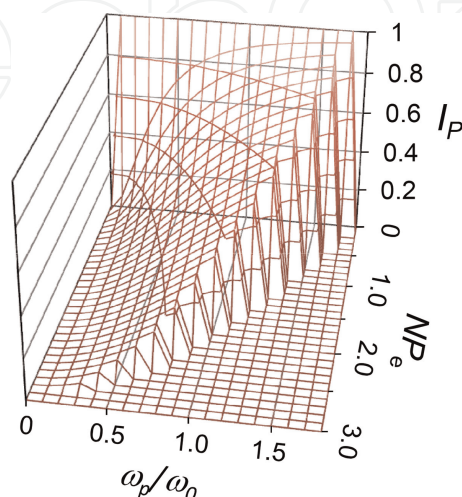


Figure 12.

Three dimensional view of the behavior of the ionicity contribution (I_P) to low-frequency dielectric constant in the plane of NP_e and ω_p/ω_0 . (ref. [25]).

this involves the contributions of both electronic (NP_e) and ionic (ω_p/ω_0) contributions, as is shown in **Figure 11a** and **Figure 11b**. Similarly, λ_0^2 corresponds to $1/\omega_T^2$, and this also involves both contributions. In contrast, it is indicated in **Figure 11** that as the electronic and ionic susceptibility amplitudes increase, the THz dielectric constant is enhanced and the softening of the characteristic resonant frequency becomes severer. These effects are strengthened significantly as the total susceptibility

$(NP_e + (\omega_p/\omega_0)^2)$ comes closer to the catastrophic limit equal to 3, at which ε_∞ diverges to infinity and ω_T/ω_0 becomes zero. This unique feature is very useful for distinguishing the mechanism of dielectric constant enhancement in different glasses. Large ε_s enhancement in ZNbKLSNd glass is primarily due to the significantly large electronic polarizability together with a reasonably high ionicity, which makes its location in NP_e - ω_T/ω_0 plane considerably close to the catastrophic boundary. On the other hand, in the case of PbNKLSNd glasses, although the ionicity ($I_P = 0.515 - 0.572$) is much higher than for ZNbKLSNd glass ($I_P = 0.465 - 0.476$), the electronic polarizability is smaller, and the overall susceptibility is not very close to the catastrophic boundary, resulting in a limited enhancement of ε_s . Fused silica has small polarizability and small ionicity ($I_P = 0.437$), and exhibits correspondingly small ε_s . La:chalcogenide glasses (S1 and S5) included in **Figure 11** for reference are considered to be highly covalent, and their enhancement in ε_s is primarily due to their electronic polarizability effect rather than the ionicity, which is consistent with their optical dielectric constant ε_∞ much higher than other glasses (See **Table 2**). Dielectric properties of other glasses are also interpreted by referring to their locations in the NP_e - ω_T/ω_0 plane.

Thus, the interplay between the electronic polarizability and ionicity determines the dielectric constant enhancement, and this feature is clearly visualized in the present analysis based on a precise single oscillator model. Physical origin of the differences found in g and λ_o^2 behaviors in **Figure 11** has been clarified by this analysis. By combining these results with other microscopic/macroscopic analyses, more detailed physical/chemical properties can be explored. Characterization on some more properties such as the electronegativity [25], bandgap energy [48] and infrared absorption spectra [30] is discussed in our recent publications.

4. Conclusion

Newly developed OFS glasses have been characterized by using THz-TDS technique, and the highest THz dielectric constant (max. 13.7) and lowest THz absorption loss (min. 5.6 cm^{-1}) in a series of multi-component silicate oxide glasses have been demonstrated. It has been shown from the frequency dependence of the absorption that the structural disorder-originated charge fluctuation are suppressed in the present OFS glasses presumably due to fluorine's structural relaxing effect, resulting in the lowest absorption even for the highest dielectric constant in ZNbKLSNd glass. Analysis based on a simplified single oscillator model has shown that ZNbKLSNd glass exhibits oscillator parameters significantly different from those of PbNKLSNd glasses as well as of other silicate oxide glasses. A unified analysis method based on a more precise single oscillator dielectric model, which can distinguish the electronic and ionic contributions, has been developed and applied to further characterization. Along with this unified model, the polarization ionicity parameter has been introduced and

confirmed to be a useful parameter to indicate the material's ionicity. The dielectric constant enhancement found in the silicate oxide glasses including OFS glasses has been systematically interpreted by the interplay between the electronic polarizability and material's ionicity. Unique properties of ZNbKLSNd glasses have been attributed primarily to their highest electronic polarizability. In contrast, the ionicity has been found to be more influential to enhance the dielectric constant in PbNKLSNd glasses. The present dielectric property analysis method based on THz-TDS technique provides a powerful tool for characterizing detailed physical nature of a variety of materials.

Acknowledgements

The authors are thankful to Ministry of Science and Technology (National Council of Science and Technology), Taiwan, for funding support to the present research (# MOST 106-2112-M-007-022-MY2, # MOST 110-2923-E-007-006). Doddoji Ramachari is thankful to Ministry of Science and Technology, Taiwan for the Post-doctoral Fellowship award during this research work. The authors thank Chao-Kai Wang and Chun-Ling Yen for their support in the THz-TDS measurements. Osamu Wada thanks to Japan Society for the Promotion of Science (JSPS KAKENHI Grant Number JP19K04532) for supporting this publication.

Conflict of interest

The authors declare no conflict of interest.

IntechOpen

Author details

Osamu Wada^{1,2*}, Doddoji Ramachari^{3,4}, Chan-Shan Yang^{5,6}, Takashi Uchino⁷
and Ci-Ling Pan¹

1 Department of Physics, National Tsing Hua University, Hsinchu, Taiwan

2 Office for Academic and Industrial Innovation, Kobe University, Kobe, Japan

3 Institute of Research and Development, Duy Tan University, Da Nang, Vietnam

4 Faculty of Natural Sciences, Duy Tan University, Da Nang, Vietnam


5 Institute and Undergraduate Program of Electro-Optical Engineering, National Taiwan Normal University, Taipei, Taiwan

6 Micro/Nano Device Inspection and Research Center, National Taiwan Normal University, Taipei, Taiwan

7 Graduate School of Science, Kobe University, Kobe, Japan

*Address all correspondence to: fwga3962@nifty.com

IntechOpen

© 2023 The Author(s). Licensee IntechOpen. This chapter is distributed under the terms of the Creative Commons Attribution License (<http://creativecommons.org/licenses/by/3.0>), which permits unrestricted use, distribution, and reproduction in any medium, provided the original work is properly cited. 

References

- [1] Grischkowsky D, Keiding S, van Exter M, Fattinger C. Far-infrared time-domain spectroscopy with terahertz beams of dielectrics and semiconductors. *Journal of Optical Society of America B*. 1990;7:2006-2015. DOI: 10.1364/JOSAB.7.002006
- [2] Tonouchi M. Cutting-edge terahertz technology. *Nature Photonics*. 2007;1:97-105. DOI: 10.1038/nphoton.2007.3
- [3] Yun-Shik Lee, *Principles of Terahertz Science and Technology*. New York: Springer; 2009. DOI: 10.1007/978-0-387-09540-0
- [4] Zhang X-C, Xu J-Z. *Introduction to THz wave photonics*. New York: Springer; 2010. DOI: 10.1007/978-1-4419-0978-7
- [5] Kai-Erik Peiponen J, Zeitler A, Kuwata-Gonokami M, editors. *Terahertz Spectroscopy and Imaging*. Heidelberg: Springer; 2013. DOI: 10.1007/978-3-642-29564-5
- [6] Bolivar PH, Brucherseifer M, Rivas JG, Gonzalo R, Ederra I, Reynolds AL, et al. Measurement of the dielectric constant and loss tangent of high dielectric-constant materials at terahertz frequencies. *IEEE Transactions on Microwave Theory and Techniques*. 2003;51:1062. DOI: 10.1109/TMTT.2003.809693
- [7] Yang C-S, Chang C-M, Chen P-H, Yu P, Pan C-L. Broadband terahertz conductivity and optical transmission of indium-tin-oxide (ITO) nanomaterials. *Optics Express*. 2013;21:16670. DOI: 10.1364/OE.21.016670
- [8] Beard MC, Turner GM, Schmuttenmaer CA. Subpicosecond carrier dynamics in low-temperature grown GaAs as measured by time-resolved terahertz spectroscopy. *Journal of Applied Physics*. 2001;90:5915. DOI: 10.1063/1.1416140
- [9] Naftaly M, Miles RE. Terahertz time-domain spectroscopy for material characterization. *Proceedings of IEEE*. 2007;95:1658. DOI: 10.1109/JPROC.2007.898835
- [10] Yang C-S, Lin C-J, Pan R-P, Que CT, Yamamoto K, Tani M, et al. The complex refractive indices of the liquid crystal mixture E7 in the terahertz frequency range. *Journal of Optical Society of America B*. 2010;27:1866. DOI: 10.1364/JOSAB.27.001866
- [11] Jepsen PU, Cooke DG, Koch M. Terahertz spectroscopy and imaging – Modern techniques and applications. *Laser Photonics Reviews*. 2011;5:124. DOI: 10.1002/lpor.201000011
- [12] Naftaly M, Miles RE. Terahertz time-domain spectroscopy of silicate glasses and the relationship to material properties. *Journal of Applied Physics*. 2007;102(4):043517/1-6. DOI: 10.1063/1.2771049,043517/1-6
- [13] Parrott EPJ, Axel J, Zeitler G, Simon B, Hehlen LF, Gladden SN, et al. Atomic charge distribution in sodosilicate glasses from terahertz time-domain spectroscopy. *Physical Review B*. 2010;82(14):140203/1-4. DOI: 10.1103/PhysRevB.82.140203
- [14] Kang SB, Kwak MH, Park BJ, Kim S, Ryu H-C, Chung DC, et al. Optical and dielectric properties of chalcogenide glasses at terahertz frequencies. *ETRI Journal*. 2009;31(6):667-674. DOI: 10.4218/etrij.09.1209.0028

- [15] Zalkovskij M, Bisgaard CZ, Novitsky A, Malureanu R, Savastru D. Ultrabroadband terahertz spectroscopy of chalcogenide glasses. *Applies Physics Letters*. 2012;**100**(3):031901/1-4. DOI: 10.1063/1.3676443
- [16] Ravagli A, Naftaly M, Craig C, Weatherby E, Hewak DW. Dielectric and structural characterisation of chalcogenide glasses via terahertz time-domain spectroscopy. *Optical Materials*. 2017;**69**:339-343. DOI: 10.1016/j.optmat.2017.04.057
- [17] Jha A. *Inorganic Glasses for Photonics: Fundamentals, Engineering and Applications*. West Sussex: John Wiley & Sons; 2016. DOI: 10.1002/9781118696088
- [18] Tanaka K, Shimakawa K. *Amorphous Chalcogenide Semiconductors and Related Materials*. New York: Springer; 2011. DOI: 10.1007/978-1-4419-9510-0
- [19] Ramachari D, Moorthy LR, Jayasankar CK. Optical absorption and emission properties of Nd³⁺-doped oxyfluorosilicate glasses for solid state lasers. *Infrared Physics and Technology*. 2014;**67**:555-559. DOI: 10.1016/j.infrared.2014.09.020
- [20] Viswanath CSD, Krishnaiah KV, Jayasankar CK. Luminescence properties of europium doped oxyfluorosilicate glasses for visible light devices. *Optical Materials*. 2018;**83**:348. DOI: 10.1016/j.optmat.2018.05.057
- [21] Manasa P, Ramachari D, Kaewkhao J, Meejitpaisan P, Kaewnuam E, Joshi AS, et al. Studies of radiative and mechanical properties of Nd³⁺-doped lead fluorosilicate glasses for broadband amplification in a chirped pulse amplification based high power laser system. *Journal of Luminescence*. 2017;**188**:558-566. DOI: 10.1016/j.jlumin.2017.04.065
- [22] Zalkovskij M, Strikwerda AC, Iwaszczuk K, Popescu A, Savastru D, Malureanu R, et al. Terahertz-induced Kerr effect in amorphous chalcogenide glasses. *Applied Physics Letters*. 2013;**103**:221102. DOI: 10.1063/1.4832825
- [23] Ramachari D, Yang C-S, Wada O, Uchino T, Pan C-L. High-refractive index, low-loss oxyfluorosilicate glasses for sub-THz and millimeter wave applications. *Journal of Applied Physics*. 2019;**125**(15):151609/1-8. DOI: 10.1063/1.5083091
- [24] Wada O, Ramachari D, Yang C-S, Uchino T, Pan C-L. High refractive index properties of oxyfluorosilicate glasses and a unified dielectric model of silicate oxide glasses in sub-terahertz frequency region. *Optical Materials Express*. 2020;**10**(2):607-621. DOI: 10.1364/OME.382686
- [25] Wada O, Ramachari D, Yang C-S, Uchino T, Pan C-L. Systematic characterization of THz dielectric properties of multi-component glasses using unified oscillator model. *Optical Materials Express*. 2021;**11**(3):858-874. DOI: 10.1364/OME.417771
- [26] Yang C-S, Lin M-H, Chang C-H, Yu P, Shieh J-M, Shen C-H, et al. Non-drude behavior in indium-tin-oxide nanowhiskers and thin films investigated by transmission and reflection THz time-domain spectroscopy. *IEEE Journal of Quantum Electronics*. 2013;**49**(8):677-690. DOI: 10.1109/JQE.2013.2270552
- [27] Parrott EPJ, Fischer BM, Gladden LF, Zeitler JA, Jepsen PU. Terahertz spectroscopy of crystalline and non-crystalline solids, chap. 8. In: Kai-Erik Peiponen J, Zeitler A, Kuwata-

Gonokami M, editors. Terahertz Spectroscopy and Imaging. Heidelberg: Springer; 2013. DOI: 10.1007/978-3-642-29564-5

[28] Roux J-F, Garet F, Coutaz J-L. Principles and applications of THz time domain spectroscopy, chap. 8. In: Perenzoni M, Paul DJ, editors. Physics and Applications of Terahertz Radiation. Dordrecht: Springer; 2014. DOI: 10.1007/978-94-007-3837-9

[29] Kuzmany H. Solid-State Spectroscopy - an Introduction. Berlin: Springer; 1998. DOI: 10.1007/978-3-662-03594-8

[30] Wada O, Ramachari D, Yang C-S, Harada Y, Uchino T, Pan C-L. Mechanism of THz dielectric constant enhancement in multi-component oxide glasses investigated by infrared and THz spectroscopies. Journal of Physics and Chemistry of Solids. 2023; **176**:111237. DOI: 10.1016/j.jpics.2023.111237

[31] Strom U, Hendrickson JR, Wagner RI, Taylor PC. Disorder-induced far infrared absorption in amorphous materials. Solid State Communications. 1974;**15**:1871. DOI: 10.1016/0038-1098(74)90106-9

[32] Strom U, Taylor PC. Temperature and frequency dependences of the far-infrared and microwave optical absorption in amorphous materials. Physical Review B. 1977;**16**:5512. DOI: 10.1103/PhysRevB.16.5512

[33] Pacewicz A, Cimek J, Salki B, Walczakowski M, Buczynski R. Reconstruction and modeling of the complex refractive index of nonlinear glasses from terahertz to optical frequencies. Optics Express. 2021;**29**(16): 26191. DOI: 10.1364/OE.431430

[34] WebElements [Internet] Available from: <https://www.webelements.com> [Accessed: February 20, 2023].

[35] Kittel C. Introduction to Solid State Physics. 8th ed. New York: John Wiley and Sons; 2005. Chap. 16

[36] Hosono H, Mizuguchi M, Skuja L. Fluorine-doped SiO₂ glasses for F₂ excimer laser optics: Fluorine content and color-center formation. Optics Letters. 1999;**24**:1549. DOI: 10.1364/OL.24.001549

[37] Duncan TM, Douglass DC, Csencsits R, Walker KL. Study of fluorine in silicate glass with ¹⁹F nuclear magnetic resonance spectroscopy. Journal of Applied Physics. 1986;**60**:130. DOI: 10.1063/1.337675

[38] Funabiki F, Kamiya T, Hosono H. Doping effects in amorphous oxides. Journal of Ceramic Society of Japan. 2012;**120**:447. DOI: 10.2109/jcersj2.120.447

[39] Wooten F. Optical Properties of Solids. New York: Academic Press; 1972. DOI: 10.11316/butsuri1946.28.9.803

[40] Fox M. Optical Properties of Solids. New York: Oxford University Press; 2001

[41] Wood RW. Physical Optics. 3rd ed. New York: Macmillan; 1934. p. 486

[42] Takebe H, Fujino S, Morinaga K. Refractive-index dispersion of tellurite glasses in the region from 0.40 to 1.71 μm . Journal of the American Ceramic Society. 1994;**77**(9):2455-2457. DOI: 10.1111/j.1151-2916.1994.tb04621.x

[43] Ibach H, Lüth H. Solid-State Physics - an Introduction to Principles of Materials Science. Berlin: Springer; 2009. Chap. 11.

[44] Grosso G, Parravicini GP. *Solid State Physics*. 2nd ed. Amsterdam: Elsevier; 2014. Chap. 9.

[45] Ashcroft NW, Mermin ND. *Solid State Physics*. Andover: Cengage learning Ltd.; 1976. Chap. 27.

[46] Wang S. *Solid State Electronics*. New York: McGraw-Hill; 1966. Chap. 7

[47] Grosse P. *Freie Elektronen in Festkoerpern*. Berlin: Springer; 1979. Japanese translation by A. Kinbara and M. Mizuhashi, *Dennshibussei no kiso*. Tokyo: Ohmsha; 1993. Chap. 13. DOI: 10.1007/978-3-642-95344-6

[48] Wada O, Ramachari D, Yang C-S, Pan C-L. Interrelationship among dielectric constant, energy band parameters and ionicity in multi-component oxide glasses revealed by optical- and THz-band spectroscopy. *Journal of Non-Crystalline Solids*. 2021; 573:121135/1–10. DOI: 10.1016/j.jnoncrysol.2021.121135